nature neuroscience

Correlated input reveals coexisting coding schemes in a sensory cortex

Luc Estebanez[1–3], Sami El Boustani[1,3], Alain Destexhe[1] & Daniel E Shulz[1]

As in other sensory modalities, one function of the somatosensory system is to detect coherence and contrast in the environment. To investigate the neural bases of these computations, we applied different spatiotemporal patterns of stimuli to rat whiskers while recording multiple neurons in the barrel cortex. Model-based analysis of the responses revealed different coding schemes according to the level of input correlation. With uncorrelated stimuli on 24 whiskers, we identified two distinct functional categories of neurons, analogous in the temporal domain to simple and complex cells of the primary visual cortex. With correlated stimuli, however, a complementary coding scheme emerged: two distinct cell populations, similar to reinforcing and antagonist neurons described in the higher visual area MT, responded specifically to correlations. We suggest that similar context-dependent coexisting coding strategies may be present in other sensory systems to adapt sensory integration to specific stimulus statistics.

Rodents acquire tactile information on objects through multiple simultaneous contacts with their whiskers[1], the results of which are encoded in the neural activity throughout the somatosensory pathway. Regardless of such multi-whisker behaviors, sensory receptive fields in the primary somatosensory barrel cortex have classically been characterized by measuring neurons' firing rates in response to sequential single whisker deflections[2]. The resulting receptive fields are defined spatially and typically include a principal whisker that produces a strong response and a few adjacent whiskers that evoke weaker responses. However, at the subthreshold level, neurons in the barrel cortex can exhibit membrane potential fluctuations elicited by whiskers well beyond the classical receptive field[3–5], suggesting that a rich functional repertoire could be revealed by coordinated whisker deflections across the whisker pad. In particular, the dynamics of whisker deflections can greatly change when whiskers touch different textures or objects in the environment[6,7], resulting in global statistics at the scale of the whisker pad that may alter the functional properties of individual neurons.

Multi-whisker motion can result in response suppression or facilitation of the principal whisker response. For instance, if the principal whisker and an adjacent whisker are deflected with a short delay (on the order of few milliseconds), the sensory response can be facilitated compared to stimulation of just the principal whisker[8,9], whereas longer delays elicit strong suppression[8–10]. Similarly the number and location of deflected whiskers can also determine whether suppression or facilitation occurs[11–13]. These studies have provided a complex and sometimes contradictory phenomenology of sensory responses for specific sets of multi-whisker stimuli. Thus, although inter-whisker nonlinear interactions have been hypothesized to be involved in the detection of whisker pad–wide stimulus contrast and coherence[9–14], the manner in which somatosensory cortex neurons encode these features remains unknown.

We investigated the effect of inter-whisker correlation at the scale of the whisker pad with a novel multi-whisker stimulator that could deliver simultaneous tactile stimuli of various profiles to the 24 caudal whiskers of rats (**Fig. 1a**) while recording multiple single units in the primary somatosensory barrel cortex. On the basis of spike-triggered analysis for various levels of inter-whisker correlation, we suggest a comprehensive framework that not only accounts for most of the previous phenomenology, but also provides a physiological role for this functional selectivity in terms of local contrast and global motion detection.

RESULTS

To assess neuronal responses for different levels of inter-whisker correlation, we used a model-based analysis that consists of deriving linear-nonlinear models from the spike-triggered covariance (STC) analysis of the recorded spiking activity[15] while stimulating all whiskers simultaneously with correlated Gaussian white noise (**Fig. 1a** and **Supplementary Fig. 1**). Linear-nonlinear models are mathematical formalisms that are widely used to characterize the functional response of neurons in sensory areas[16]. These computational models describe the functional relationship between sensory stimuli and the output firing rate of neurons in two steps. First, the stimulus is projected onto the subspace of the stimulus ensemble that produces significant changes in the neuron's firing rate. This subspace is defined by vectors acting as linear filters. Second, a nonlinear function provides an estimate of the neuron firing rate as a function of stimulus location in the subspace identified in the first step. Overall, this analysis reveals the spatio-temporal features of the stimulus that determine the spiking activity of the recorded neuron.

A shared two-dimensional phase space in barrel cortex

Using this formalism, we first identified the stimulus subspace to which barrel cortex neurons are sensitive (first stage of the

[1]Unité de Neurosciences, Information et Complexité, UPR 3293, Centre National de la Recherche Scientifique, Gif sur Yvette, France. [2]Institut de Biologie de l'École Normale Supérieure, Institut National de la Santé et de la Recherche Médicale U1024, Centre National de la Recherche Scientifique UMR8197, Paris, France. [3]These authors contributed equally to this work. Correspondence should be addressed to A.D. (destexhe@unic.cnrs-gif.fr) or D.E.S. (shulz@unic.cnrs-gif.fr).

Received 18 April; accepted 11 October; published online 18 November 2012; doi:10.1038/nn.3258

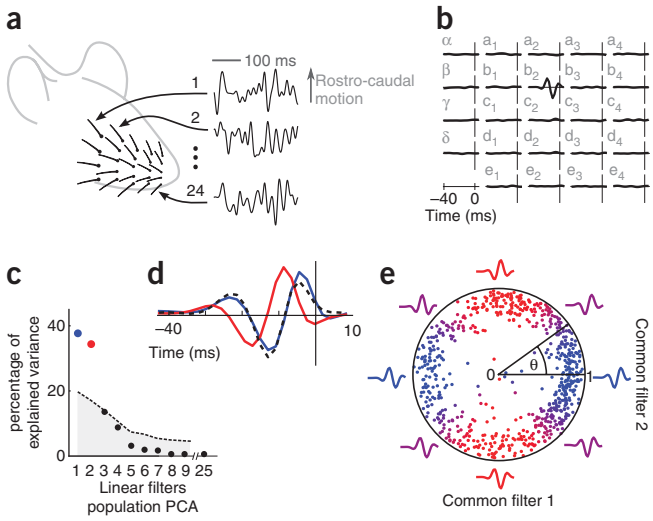

Figure 1 Barrel cortex neurons encode whisker deflections in a common low-dimensional subspace. (**a**) Uncorrelated Gaussian white noise was applied to 24 whiskers on the rat right whisker pad in the rostro-caudal axis. (**b**) Example of a significant linear filter showing whisker displacement over time for a mono-vibrissal neuron obtained using STC analysis. (**c**) PCA over all significant linear filters obtained among all protocols for mono-vibrissal neurons (680 filters), with two dominant eigenvalues explaining 73% of the variance (blue and red points). Dashed line represents mean + three s.d. significance threshold. (**d**) Corresponding common filters, together with the Hilbert transform of the red filter (black dashed line). (**e**) Normalized significant filters of all neurons and protocols, projected onto the stimulus subspace spanned by the common filters. The radius corresponds to the similarity of the individual filter with common filters 1 and 2.

linear-nonlinear model). All neurons were recorded in layers with sufficient spiking activity[17], namely layers IV, V and VI a prerequisite for carrying out STC analysis. During the different Gaussian noise whisker stimulations used for reverse correlation analysis (**Supplementary Table 1**), 28% (N = 429/1530) of the units displayed significant linear filters for at least one protocol, as computed by the z score obtained with surrogate data (Online Methods). Among these 429 responsive neurons, 344 displayed significant linear filters specifically in response to uncorrelated stimulations. Most of these significant linear filters were limited to a single whisker (83%, N = 286 of 344 neurons; **Fig. 1b**), whereas a subset of neurons displayed significant responses to more than one whisker (two whiskers, 13%; three whiskers, 4%). In these cases, the filters of adjacent whiskers were generally antagonists to the principal whisker (data not shown).

Across all stimulation conditions (including stimuli with different levels of inter-whisker correlation), significant linear filters were very similar across neurons, as seen in their frequency content (average of ~53 Hz, much below the input cut-off frequency; **Supplementary Figs. 2** and **3**), suggesting the existence of a low-dimensional spike-triggered subspace common to all neurons. To extract linear filters common to all responding neurons, we performed a principal component analysis (PCA) across all of the significant individual whisker linear filters that we obtained with the STC analysis. Notably, only the first two principal components were larger than three standard deviations from a randomized control distribution (**Fig. 1c** and Online Methods). These two common filters were sufficient to explain 73% of the variance of the 680 monovibrissal linear filters (N = 371) that were obtained during the different reverse correlation protocols (**Fig. 1c**,**d**).

A similarly low-dimensional sensory subspace, also described by two common filters with a 0.8-Hz preferred frequency, has been reported in the locust antenna lobe[18]. However, the two filters found here were 90° de-phased versions of each other. This de-phasing was made clear by comparing the Hilbert transform of common filter 2 (corresponding to a 90° de-phasing; **Fig. 1d**) to common filter 1. This de-phasing was also present at the level of individual neurons filters (**Supplementary Fig. 4b**), indicating that individual neurons are tuned to whisker phases at an average frequency of 53 Hz.

To ensure that individual filters were all equally explained by the common filters, we projected a normalized version of all of these filters on the two-dimensional subspace defined by the common filters (**Fig. 1e**). In this subspace, the distance from the origin indicates the degree to which the individual filters are explained by the common filters subspace. Notably, all projections lay close to the unit circle, indicating that the corresponding filters were adequately described in this common subspace (there was no additional cluster of poorly explained filters; **Supplementary Fig. 4c**).

We also verified that the phase space was not a projection in the rostro-caudal axis of the classical directional selectivity in the ventro-dorsal and rostro-caudal plane[2]. In a subset of neurons (n = 33), we were only able to poorly predict individual neuron rostro-caudal phase tuning from the directional tuning in the rostro-caudal and ventro-dorsal plane (21% of explained variance; **Supplementary Fig. 5c**) or from the rostro-caudal axis alone (30% of explained variance). This suggests that the phase is itself a coding property and cannot be systematically predicted by the classical directional space.

We used this phase subspace to conveniently represent the functional response of the studied neurons in the rostro-caudal axis in terms of the phase of whisker deflections with respect to a common preferred frequency. This common space can also be interpreted in terms of tuning to whisker position and speed as well as any linear combination of these two properties. Indeed, although common filter 1 is comparable to a differentiator filter selective for whisker deflection speed, common filter 2 is closer to a unidirectional filter, mainly selective for the whisker position (**Supplementary Fig. 6**).

Simple and complex responses to uncorrelated stimulations

Having identified the common phase subspace of the neuronal response, we evaluated the selectivity of the neuronal response in this space. For all neurons, we computed the second stage of the linear-nonlinear model, the nonlinear function (**Fig. 2a**,**b**). The nonlinear function is an estimate of the neuron firing rate in response to an arbitrary stimulus after it has been projected into the common subspace. It provides an estimate of the neuron firing rate across phases.

This computation was first performed for the response to an uncorrelated stimulus, meaning that the 24 whiskers were deflected simultaneously, but in a non-coordinated manner. This analysis was performed only on neurons that responded significantly to a single whisker (N = 286 out of 344 neurons responsive to uncorrelated stimulations), as these cells could be directly described in the two-dimensional common subspace. Because of their localized receptive field, we refer to these neurons as local neurons. Under uncorrelated stimulation conditions, these neurons showed two types of neuronal responses in the temporal domain. First, 29% (N = 82 of 286 neurons) of the local neurons responded selectively to a single phase of the common subspace and were therefore accurately described by a single significant linear filter along this dimension followed by a one-dimensional directional-selective nonlinearity (**Fig. 2a**). Second, all of the other responding neurons (71%) featured a broad phase tuning spanning most of the common

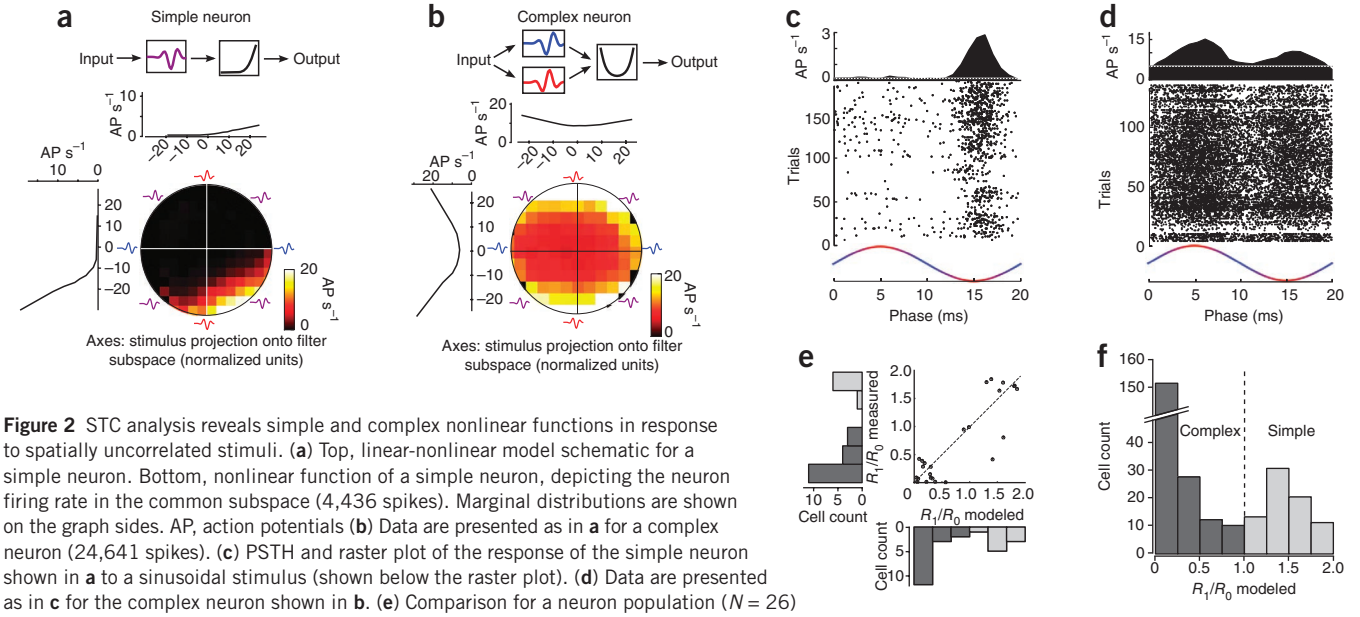

Figure 2 STC analysis reveals simple and complex nonlinear functions in response to spatially uncorrelated stimuli. (**a**) Top, linear-nonlinear model schematic for a simple neuron. Bottom, nonlinear function of a simple neuron, depicting the neuron firing rate in the common subspace (4,436 spikes). Marginal distributions are shown on the graph sides. AP, action potentials (**b**) Data are presented as in **a** for a complex neuron (24,641 spikes). (**c**) PSTH and raster plot of the response of the simple neuron shown in **a** to a sinusoidal stimulus (shown below the raster plot). (**d**) Data are presented as in **c** for the complex neuron shown in **b**. (**e**) Comparison for a neuron population ($N = 26$) between the modulation index R_1/R_0 measured using sinusoidal stimulus (ordinate) and the prediction derived from the linear-nonlinear models (abscissa). (**f**) Population histogram of the modulation index R_1/R_0 as predicted from all recorded local neurons using their linear-nonlinear models ($N = 286$).

subspace. Such neuronal responses were accurately described by a model that included the two dimensions spanned by the common filters and quadratic nonlinear functions (**Fig. 2b**). These two functional cell types have been reported previously in the barrel system, in which identical Gaussian noise was applied to all whiskers simultaneously[19]. Consistent with this previous study, we referred to these neurons as simple and complex because of their clear resemblance in the temporal domain to simple and complex neurons in the primary visual cortex (V1).

Such a comparison was supported by their response to periodic stimulations, in which vertical gratings composed of 50-Hz sinusoidal stimuli were applied on all whiskers, with opposite phase in every adjacent whisker arc, that is, a stimulus that mimics in space and time the drifting gratings that are classically used to differentiate simple and complex neurons in V1 (ref. 20). As predicted by the linear-nonlinear model, simple neurons firing was phase-locked with a sharp tuning to one phase of the sinusoidal stimulus (**Fig. 2c**), whereas complex neurons displayed a global increase of firing rate with either phase doubling (**Fig. 2d**) or no modulation.

From these peristimulus time histograms (PSTHs), we derived the index of modulation, R_1/R_0 (Online Methods). This index, which is used to differentiate simple and complex cells in V1 (ref. 20), clustered our simple and complex neurons into two groups that were predicted by the linear-nonlinear models ($N = 26$; **Fig. 2e**). To better estimate the population simple and complex neuron distribution, we also applied this analysis to all neurons for which we could estimate a linear-nonlinear model. This population analysis also resulted in a bimodal distribution (**Fig. 2f**). In addition, consistent with our V1 comparison, we observed that the baseline firing rates of complex neurons were significantly higher on average than the firing rates of simple neurons (Mann-Whitney P value = 10^{-9}; see **Supplementary Fig. 7h**,**i**), consistent with the classical description of these two functional types in the visual system[21].

In experiments supported by histological analysis ($N = 159$), we found no simple neurons in the thalamo-recipient compartment, the barrels of layer IV ($N = 14$), whereas we did find a large number of simple neurons in the septa ($N = 13$) that surrounds the barrels (**Supplementary Fig. 8c**). This measurement indicates that simple neurons are found in lower proportion in barrels than in septa, which is consistent with the higher directional selectivity that has been reported in septa versus barrels[3,22], but is at odds with the large proportion of simple neurons that have been reported in layer IV of the primary visual cortex.

Local and global responses to spatial correlation

To determine whether the simple and complex dichotomy established using uncorrelated noise was sufficient to capture barrel cortex functional responses even for different stimulus statistics, we recomputed the linear-nonlinear model for different levels of spatial coherence in the stimulus. To do so, we progressively increased the level of inter-whisker correlation from 0 to 100% by adding a common Gaussian noise to each whisker (**Fig. 3a**). Neuron responses for these correlated stimulation patterns were assessed for 222 of the 429 neurons that were analyzed with uncorrelated Gaussian noise.

Notably, the initial model with simple and complex dichotomy turned out to be insufficient, as a subpopulation of neurons that did not display any significant response during uncorrelated stimulation ($P > 0.01$, $N = 75$ of 222 neurons; **Fig. 3b**) showed significant responses with linear filters in correlated stimulation conditions ($P < 0.01$, **Fig. 3c**,**d**). Because of their specific sensitivity to motion at the whisker pad scale, we referred to these neurons as global neurons. Their response increased with correlation strength, as seen in the nonlinear function of the common subspace (**Fig. 3c**) and its marginal projections (**Fig. 3d**). This functional property may be similar to neurons sensitive to multiple whisker deflections that were found previously using multi-whisker stimulations[23].

The local neurons (responsive to a single whisker during uncorrelated stimulations) that were also recorded during correlated stimulations ($N = 147$ of 222 neurons) were inversely affected by increased levels of inter-whisker correlation, exhibiting a decrease in the nonlinear function amplitude (**Fig. 3e**,**f**). This local and global distinction was further supported by the bimodal population distribution of the statistical significance of linear filters in the uncorrelated stimulation condition for all responsive cells (**Fig. 3b**).

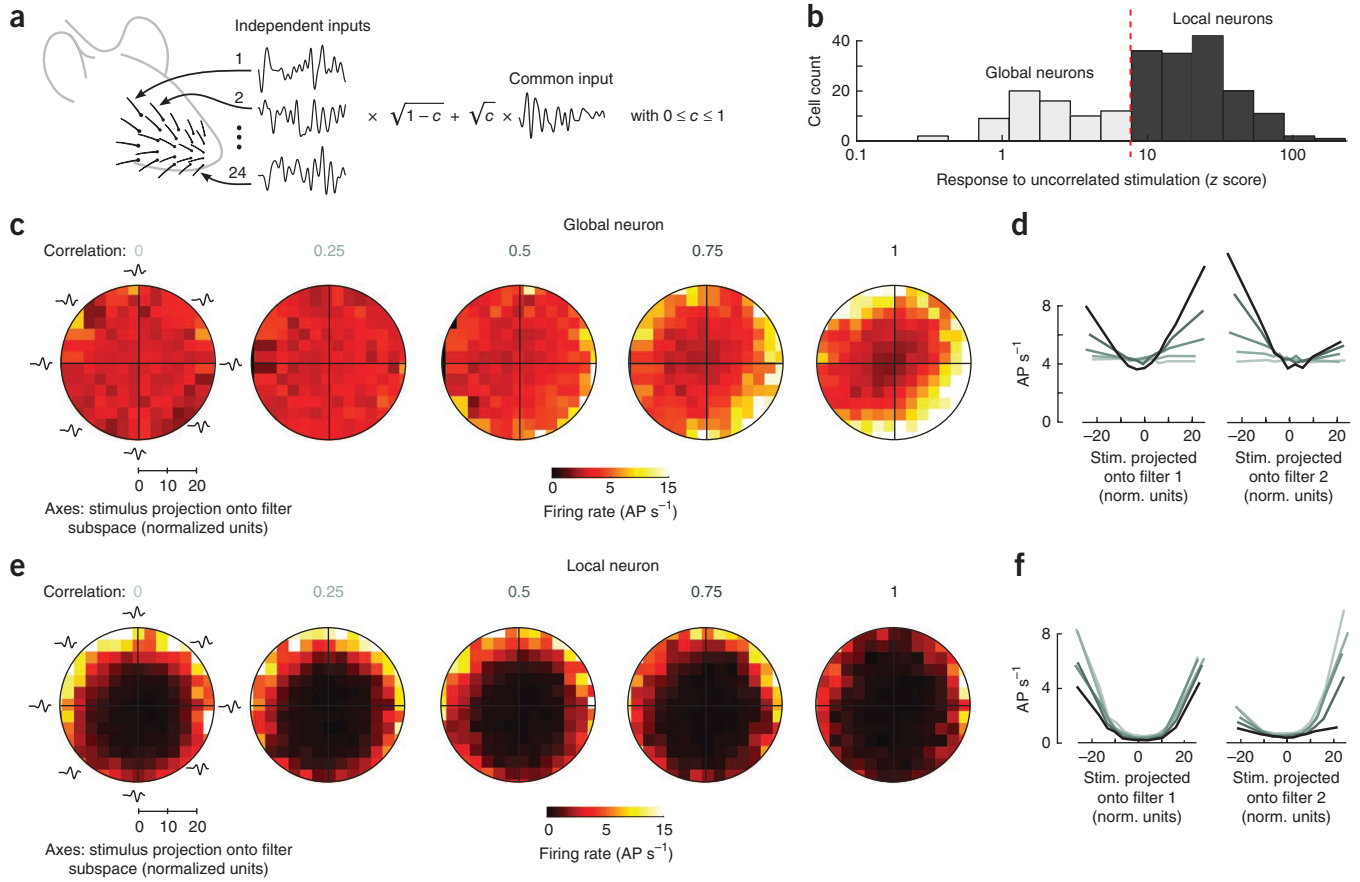

Figure 3 Neurons' nonlinear functions depend on interwhisker instantaneous correlation. (**a**) Stimuli with interwhisker correlation *c* were built by weighted summation of independent and common Gaussian noise stimulations. (**b**) The bimodal *z* score population distribution obtained with uncorrelated (and correlated) Gaussian noise defines local (dark gray) and global (light gray) neurons among all responsive neurons ($N = 222$). Red dashed line represents 1% significance threshold. (**c**) Nonlinear function of a layer V global neuron for five increasing levels of interwhisker correlation (gray to black). Spike counts from uncorrelated to correlated: 9,815, 10,148, 10,694, 10,863 and 11,089 spikes. (**d**) Marginal nonlinear functions for the different levels of correlation along common filters 1 (left) and 2 (right). (**e**,**f**) Data presented as in **c** and **d** for a layer V local neuron (spike counts from uncorrelated to correlated: 2,317, 1,968, 1,787, 1,363 and 1,040 spikes). Stim., stimuli; norm., normalized.

Both local and global neurons displayed a simple and complex dichotomy in their tuning to the phase space. Of the neurons that were tested for both correlated and uncorrelated stimulations ($N = 222$), 47% were local complex neurons ($N = 105$), 19% were local simple neurons ($N = 42$) and 31% were global complex neurons ($N = 69$). Global simple neurons were rarely seen (3%, $N = 6$). In addition, an anatomical segregation of global complex and local simple functional types was also visible in a subset of neurons for which a full histological analysis was carried out ($N = 159$; **Supplementary Fig. 8**). In particular, septa and layer VI displayed a large proportion of local simple neurons and almost no global neurons, whereas layer V and the barrels in layer IV showed almost no local simple neurons and a large proportion of global neurons. Such layered functional organization could also be seen in the distribution of functional types as a function of the electrode recording depth for all functionally responsive neurons ($N = 429$; **Supplementary Fig. 8d**) and is similar to the segregation of local and global cells found in visual area MT[24].

Center-surround antagonism in local receptive fields

To determine why the sensory responses of mono-vibrissal local neurons were affected by inter-whisker correlation, we applied a protocol that explored center-surround whisker interactions ($N = 91$). We applied one Gaussian noise stimulus to the center whisker (principal whisker) and a different Gaussian noise stimulus to all surrounding whiskers (**Fig. 4a**). We derived from this experiment a two-compartment center-surround linear-nonlinear model of the neuron, resulting in a two-dimensional tuning map describing the neuron firing rate for all center-surround phase combinations. To do so, we projected, for every spike of a given neuron, the corresponding center and surround stimulus into the common subspace. We collected the resulting joint center-surround phases (**Fig. 4a**) and built the corresponding two-dimensional tuning map by computing the histogram over all observed spikes. This map provides an estimate of the strength of a neuron response as a function of the phases of both the center and the surround stimulations, including identical or antagonist center-surround phases.

In this representation, 38% ($N = 35$ neurons of 91 tested) of the filters were tuned both to center and surround stimuli (Rayleigh test, $P < 0.05$; **Fig. 4b**). Across these tuned neurons, the distribution of the center-surround optimal phase difference peaked sharply on antagonist center-surround phases (**Fig. 4c**), providing a direct explanation for their decreased response to correlated stimulations. Indeed, this decreased response could be seen in the diagonal of the two-dimensional tuning map and could be compared with the phase tuning measured with fully correlated stimulations (**Fig. 4b**). Notably, the 'center' marginal distribution also accurately

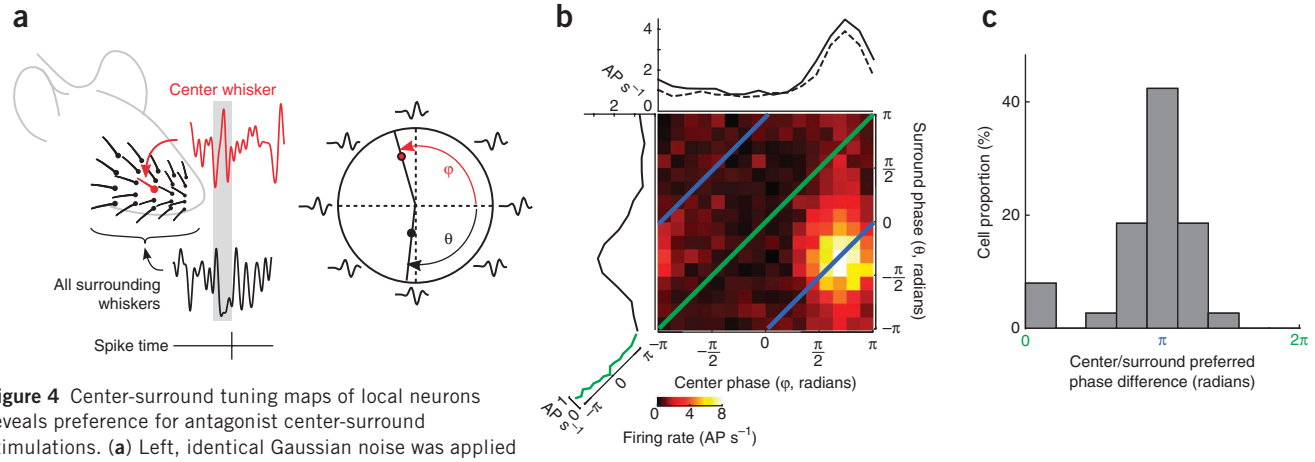

Figure 4 Center-surround tuning maps of local neurons reveals preference for antagonist center-surround stimulations. (**a**) Left, identical Gaussian noise was applied to all whiskers except the center whisker, which was stimulated with a different Gaussian noise waveform. Spike-triggered center and surround stimulus segments were collected. Right, the phase of both center and surround in the common subspace was computed for every spike and allowed the construction of a center/surround nonlinear function, the phase tuning map presented in **b**. (**b**) Center-surround phase tuning map of a simple neuron (4,159 spikes). The green line represents correlated stimuli and the blue lines represent antagonist stimuli. Left, marginal surround phase tuning. Top, marginal center phase tuning. Dashed line represents phase tuning curve obtained using uncorrelated stimulation as in **Figure 1a**. Bottom left, green tilted graph indicates phase tuning curve obtained with a fully correlated stimulation. (**c**) Population distribution of the preferred phase difference between center and surround for neurons showing a significant center and surround phase tuning ($N = 35$ of 91, Rayleigh test, $P < 0.05$).

predicted the phase tuning for uncorrelated stimulations. Indeed, center-surround–tuned simple neurons displayed a sharp center-surround tuning that resulted in a center marginal distribution with a sharp tuning to a single phase similar to the tuning curve observed with uncorrelated Gaussian noise in the center whisker (**Fig. 4b**). In contrast, center-surround–tuned complex neurons responded to a broad range of antagonist center-surround stimulations, leading to a broad tuning to the center phase in the marginal projection that matched the tuning curve obtained during uncorrelated noise (data not shown). Overall, this analysis provides a generalized model of local mono-vibrissal neurons responses across a range of stimulation statistics going from spatially uncorrelated to fully correlated.

Forward correlation confirms local and global properties

We first verified that center-surround phase tuning maps of local mono-vibrissal neurons were a correct estimation of the underlying functional properties. We used a playback protocol in which deflection profiles identical to the first common filter (**Fig. 1d**, blue) were applied (for both polarities) to the center whisker while the surround whiskers were stimulated in either a correlated (**Fig. 5a–d**, green) or anti-correlated manner (**Fig. 5a–d**, blue) or were not stimulated at all (**Fig. 5c**,**d**, red). As predicted by the phase tuning map and by **Figure 3e**,**f**, when the center whisker was deflected with the preferred phase, the PSTH resulting from correlated stimulations was weaker than that resulting from single whisker stimulation (equivalent to uncorrelated surround stimulation; **Supplementary Fig. 9**), whereas the response was strongly facilitated for center-surround antagonist stimulations (**Fig. 5d**). Outside the preferred center phase, correlated, single whisker or antagonist stimulations elicited weaker responses (**Fig. 5c**). Across the population ($N = 9$), the response to antagonist stimulations was significantly more reliable than the response to correlated ($P < 0.01$; **Fig. 5e**,**f**) or uncorrelated stimulation ($P < 0.01$; **Fig. 5f**), with values well above those previously reported for single or dual whisker stimulations[9,25]. It is worth noting that the surround modulation for these cells was bidirectional (facilitation and suppression) and did not result from the application of a dense stimulation over all whiskers. Indeed, the response amplitude obtained with uncorrelated playback over the whisker pad was similar to the response obtained when only the center whisker was stimulated (**Supplementary Fig. 9**).

The linear-nonlinear model gave good predictions of the response to these playback stimuli (**Fig. 5c**,**d** and **Supplementary Fig. 10**). To test the ability of the center-surround model to predict a neuron's functional response to a set of novel stimuli with statistics matching those encountered by the animal during its behavior, we repeatedly applied natural whisker deflections obtained using a high-speed video camera to record the movements of the whiskers when sweeping a textured surface on them (**Fig. 5g** and Online Methods). These natural whisker deflections displayed a richer temporal structure than the Gaussian white noise used to build our linear-nonlinear models, as can be seen in the respective auto-correlogram of these two stimuli (**Fig. 5h**). We applied these natural whisker stimulations in two different protocols. In one protocol, all of the whiskers were fully correlated whereas in the other the center and surround whiskers were stimulated with two different and uncorrelated natural stimuli (**Fig. 5g**,**h**). The full center-surround linear-nonlinear model predicted the response of local neurons to uncorrelated center-surround natural stimuli ($N = 16$, mean Pearson coefficient between PSTHs with a 20-ms time bins, $r = 0.50$) significantly better than a center-only linear-nonlinear model ($N = 16$, $r = 0.35$, Wilcoxon paired test, $P < 0.02$; **Fig. 5i**), demonstrating the need to include a contextual compartment (surround) in classical functional models. Moreover, using the same center-surround model, we were able to equally well predict the response of local neurons to both correlated ($N = 16$, mean Pearson coefficient = 0.51) and center-surround natural stimuli (Wilcoxon paired test, $P > 0.5$; **Fig. 5j**), thereby indicating, to some extent, the completeness of the model. Similar controls were carried out with uncorrelated playback (**Supplementary Fig. 10a–d**) and natural stimuli (**Supplementary Fig. 10e**,**f**) using the classical linear-nonlinear models (**Fig. 2**) to show the validity of the common subspace.

We also verified that the specific sensitivity of global neurons to highly correlated stimulations (**Fig. 6a**) was indeed observed when performing a similar playback protocol (**Fig. 6a**). When we applied a spatially uncorrelated playback pattern, we did not evoke a significant

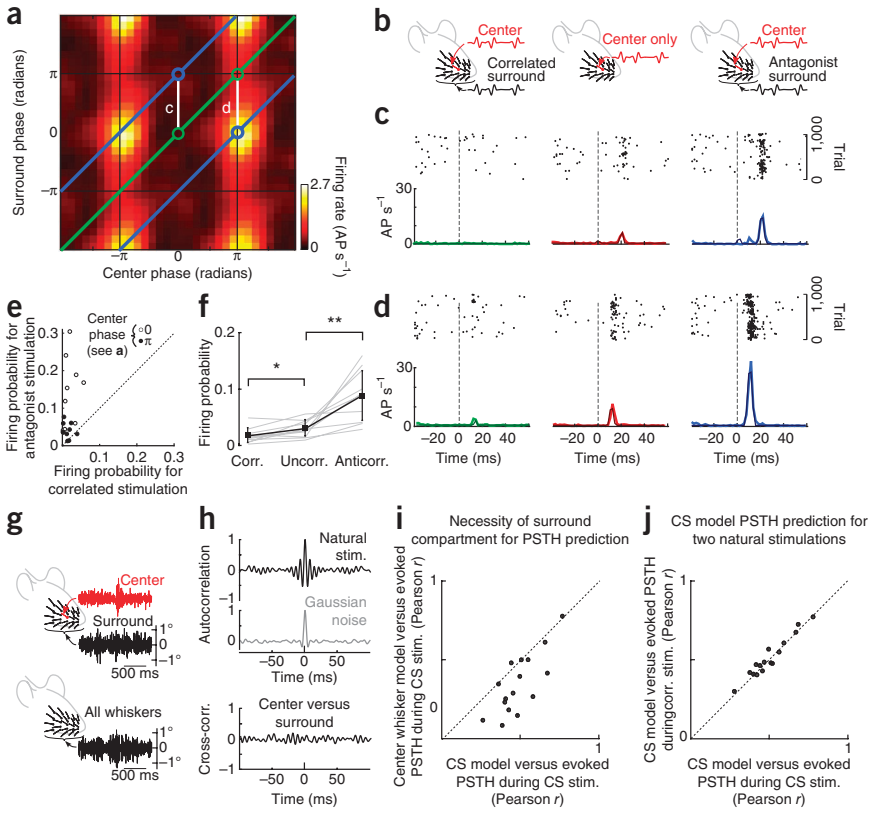

Figure 5 Confirmation of the antagonist tuning of local neurons. (**a**) Center-surround tuning map of a simple local neuron (1,216 spikes). Green and blue lines represent correlated and antagonist stimulus subspace, respectively. (**b**) Common filter 1 playback, correlated (left), antagonist (right), and center whisker only (middle). (**c**) Raster plots and corresponding PSTHs for correlated (light green), antagonist (light blue) and center-only (light red) playback. Dark curves represent corresponding linear-nonlinear model predictions. (**d**) Data presented as in **c** for opposite center phase. (**e**) Response reliability in correlated versus antagonist stimuli for two opposite center phases (c and d in **a**, $N = 9$). (**f**) Reliability for correlated (corr.), uncorrelated (uncorr.) and anti-phased (anticorr.) stimuli for the same population ($N = 9$). Uncorrelated stimulation reliability was significantly higher than correlated reliability (Wilcoxon paired test, $^{*}P < 0.05$), but significantly lower than anti-phased reliability (Wilcoxon paired test, $^{**}P < 0.01$). Error bars represent s.d. (**g**) Uncorrelated center-surround (top) and correlated (bottom) natural whisker deflections used in **i** and **j**. (**h**) Auto-correlogram of natural (top) and Gaussian (middle) stimulus (stim.). Bottom, cross-correlogram (cross-corr.) of center versus surround stimuli. (**i**) Goodness-of-fit of the natural center-surround stimulus PSTHs with a center-surround (CS) model versus center-only model ($N = 16$, Wilcoxon paired test, $P < 0.02$). (**j**) Goodness-of-fit of the PSTH recorded during the natural center-surround stimulus and during the correlated natural stimulus, using the same center-surround model (same population as in **i**, Wilcoxon paired test, $P > 0.5$).

response in most of these cells ($P > 0.05$; **Fig. 6b**). However, spatially correlated deflections resulted in strong responses, as expected for this cell type (**Fig. 6c**). This observation was confirmed across the whole population of global neurons that we tested by z score assessment (5% significance threshold, $N = 23$; **Fig. 6d**).

Finally, we correlated the global and local classification with the size of the receptive fields obtained using standard sparse noise stimulations (**Supplementary Fig. 7**). Global neurons exhibited weaker and significantly larger spatial receptive fields than local neurons (global, $N = 12$; local, $N = 16$; Mann Whitney $P = 2.7 \times 10^{-3}$), as well as significantly higher baseline firing rates (global, $N = 75$; local, $N = 147$; Mann Whitney $P = 3.0 \times 10^{-7}$). The large sparse receptive field of global neurons may be instrumental for determining their sensitivity to spatial correlation.

Center-surround delays facilitate and suppress local neurons

Previous reports have found that different interstimulus intervals (ISIs) between a principal whisker and one of its adjacent whiskers can result in either facilitation or suppression relative to the neuron response to principal whisker deflection alone[8,9,26,27]. To compare our model predictions with these findings, we examined center-surround phase tuning maps of local neurons for various delays between spike times and center (δt_{center}) or surround stimulations times ($\delta t_{surround}$) (**Fig. 7a**). The phase tuning maps computed for different δt_{center} and $\delta t_{surround}$ displayed shifts of the preferred stimulus center-surround phases (**Fig. 7b**). This suggests that the functional response to stimulations predicted by the phase tuning map for specific center-surround phase relationships depends on the delay between center and surround stimulations.

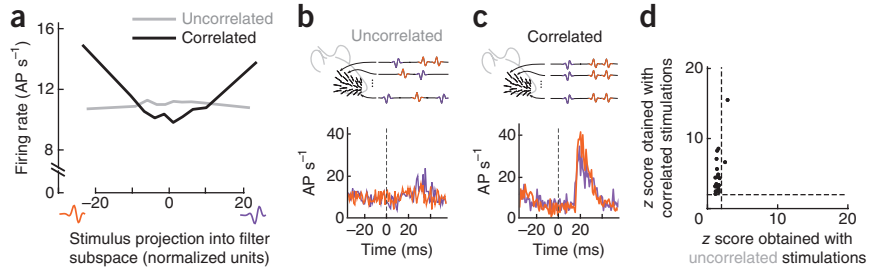

Figure 6 Confirmation of the functional properties of global neurons. (**a**) Nonlinear function (projected onto common filter 1 dimension) of a global neuron obtained during uncorrelated (gray, 26,193 spikes) and correlated (black, 26,322 spikes) stimulations. Color-coded (orange and purple) waveforms on the bottom sides of the graph indicate the direction in the filter 1 subspace (as in **b** and **c**). (**b**) Top, spatially uncorrelated playback of the first common filter in both directions (orange and purple) with an ISI drawn from a Poisson distribution (see Online Methods). Bottom, corresponding most responsive PSTH among all whiskers for both stimulus directions. (**c**) Data are presented as in **b** for a spatially correlated stimulus. (**d**) Population analysis of the PSTH z score for uncorrelated versus correlated stimulations. Dashed lines represent 5% significance thresholds.

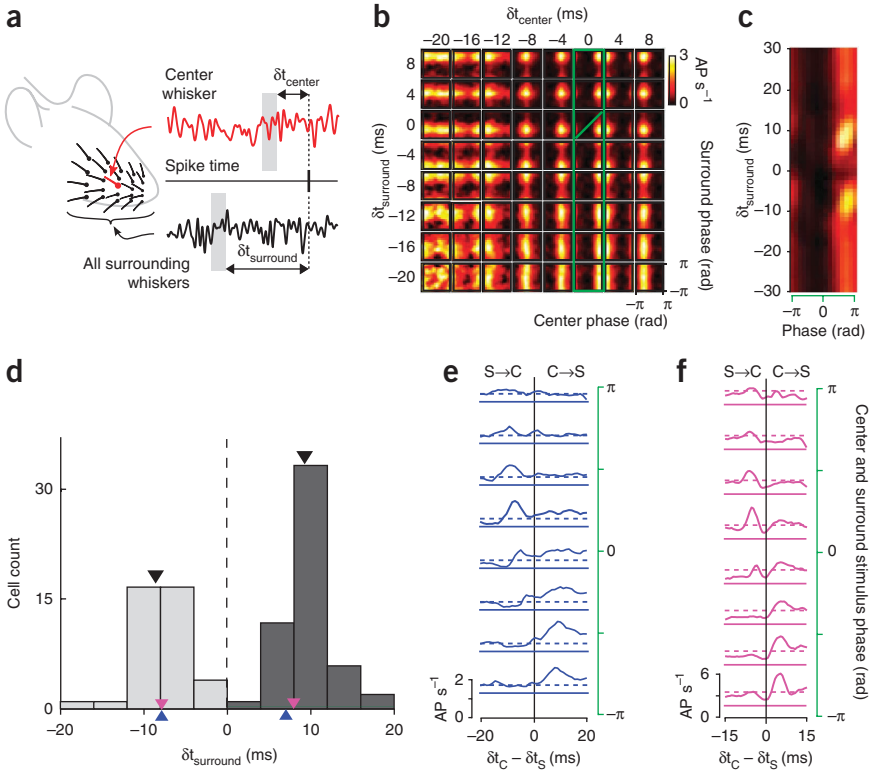

Figure 7 Center and surround phase tuning with temporal delays. (**a**) Phase tuning maps for center and surround stimulations were computed for −40-ms to +10-ms windows that were shifted with various delays between the spike time and the center (δt_{center}) or surround ($\delta t_{surround}$) stimulations. (**b**) Resulting center and surround phase tuning maps for different delays (δt_{center}, $\delta t_{surround}$) for a local simple cell (4,159 spikes). (**c**) Neuron firing rate for $\delta t_{center} = 0$ and various surround delays when considering identical center and surround stimulation phases (that is, the diagonal of the tuning map along the $\delta t_{center} = 0$ column shown in green, corresponding to correlated center-surround stimulations). (**d**) Population distribution of the significant positive ($N = 55$) and negative ($N = 40$) surround delays across all neurons that display facilitation ($N = 67$). Average negative (–8.6 ms) and positive (9 ms) delays are indicated with black arrows. The preferred delays for **e** (–8 ms and +7.6 ms) and **f** (–8 ms and +8 ms) are shown as blue and purple arrows, respectively. (**e**) Center (C)-surround (S) ISI curves derived from **b** for 16 different center and surround stimulations (tuning map diagonal in green). Continuous blue line represents baseline activity. Dashed lines represent maximal firing rate to center-only stimulations. (**f**) Data are presented as in **e** for a second case study.

We focused on the case in which center and surround stimulations share identical phases (ranging from $-\pi$ to π). We kept the center stimulus delay fixed ($\delta t_{center} = 0$) and varied the surround delay ($\delta t_{surround}$) from −30 to +30 ms (**Fig. 7c**). In this representation, 73% of the neurons studied displayed a significant surround modulation for at least one $\delta t_{surround}$, as defined by a z score 1% significance threshold. Neurons were able to display significant facilitation to positive ($N = 40$) or negative ($N = 55$) $\delta t_{surround}$ (**Fig. 7c**). These optimal surround delays were specific to each neuron, ranging from −15 to +15 ms, with population average negative shifts at −8.6 ms and positive shifts at +9 ms (**Fig. 7d**). This order of magnitude of the surround delay for the peak of facilitation is similar to the delay between adjacent whisker stimulation that resulted in the strongest tuning for the apparent direction of a front edge stimulus crossing the whisker pad[28].

Finally, to directly compare the functional properties that we obtained with previous studies of interwhisker interactions using ISI curves[8,9,26], we derived a set of eight ISI facilitation curves (**Fig. 7e**,**f**) from the delay-dependent phase tuning map (**Fig. 7b**). Each of these curves describes, for a given stimulus (applied to both the center and surround compartments), the neuronal response facilitation for a range of ISIs. We computed these curves by considering the functional responses predicted by the delay-dependent phase tuning map for each ISI at all δt_{center} and $\delta t_{surround}$ values such that $\delta t_{center} - \delta t_{surround}$ = ISI remains fixed. Each point of the curve corresponds to the maximal evoked response for a fixed ISI.

We observed in the ISI curves of many local neurons that suppression was present for 0-ms delays (**Fig. 7f**, as expected from antagonist cells) which is consistent with previously reported ISI curves[8]. Other ISI curves were dominated by facilitation for delayed center-surround stimulations, matching ISI curves from a previous study[4] (**Fig. 7e**). In that particular study, the authors also identified another set of cells that showed ISI facilitation for simultaneous deflections of the principal whisker and the adjacent whisker. These cells likely correspond to the global cells reported in our analysis.

In addition, we found that the variety of ISI curves that was found across barrel cortex neurons could be directly related to the phase tuning of these cells and was strongly stimulus dependent (**Fig. 7e**,**f**), as previously reported[26]. This analysis reveals that the center-surround tuning map representation is general enough to reproduce results obtained previously and to explain the seemingly contradictory phenomenology of context-dependent integration that has been described in the barrel cortex.

DISCUSSION

We have found that correlations in whisker stimuli markedly changed not only firing responses, but also the coding strategy used by barrel cortex neurons. With uncorrelated stimuli, a localized simple-complex type of response was observed, similar in the temporal domain to the responses typically seen in the primary visual cortex. These two types of neurons have been already reported[19], but simple cells were rarely seen, in contrast with our own observations. A direct explanation for this apparent discrepancy can be found in the manner in which all of the whiskers were deflected as a bundle in the previous study, resulting in a stimulation similar to our fully correlated protocol. Indeed, almost no global neurons were simple (3%) and most of the local simple neurons were tuned to center-surround antagonist stimulation and/or were multi-vibrissal with a principal whisker filter flanked by antagonist filters on the adjacent whiskers (data not shown). All local simple neurons, as a result of their functional properties, were therefore suppressed by correlated stimulations and were previously undersampled.

When correlations were introduced among the 24 whisker deflections, new populations of cells and new types of responses were observed. At high levels of inter-whisker correlation, we found

two populations: global neurons that encoded coherent motion at the whisker pad scale and local neurons that were tuned to center-surround local contrast. These two categories were highly similar to the reinforcing and antagonist cells described in area MT/V5 of the dorsal stream in the monkey visual cortex[24,29], a sensory area that receives thalamic sensory afferents, similar to V1 (ref. 30). This analogy is further supported by the recent discovery that the somatosensory representation of monkey fingertips may be comparable with a different facet of MT/V5 processing: vector averaging of motion[31,32]. Such high-level processing should also be considered in the context of the strong motor integration of the barrel cortex[33,34]. Indeed, MT/V5 is known to be involved in the control of pursuit eye movements that allow the retinal fovea to be kept focused on moving objects[35,36]. We expect that similar mechanisms, implemented with global and local neurons, are used to track large-scale whisker deflections to maintain whisker focus onto moving tactile objects.

We were able to obtain good response estimations from only 28% of the recorded units, making it hard to infer a full picture of the barrel cortex functional properties from our data. This is partially a result of the limitation of our exploration to the rostro-caudal deflection axis, whereas barrel cortex neurons are known to display direction selectivity for other directions of deflection too[2]. Moreover, second-order reverse correlation techniques such as the STC used here require long recordings to accumulate enough statistics[15,37]. Using forward-correlation experiments (correlated and uncorrelated playback; **Figs. 5b–d** and **6b**,**c**), which are less statistically demanding, we found that 49% of the recorded neurons displayed significant responses for correlated or uncorrelated stimulations (z score, 5% significance threshold).

Our experiments were carried out under anesthesia because observations of barrel cortex neurons responses to controlled multi-whisker stimulations would have been practically intractable in the awake rodent. The use of a light isoflurane anesthesia suppressed active whisking and twitching movements while maintaining strong sensory responses in the barrel cortex. This required the maintenance of a precise tuning of the anesthesia to low anesthetic states on the basis of electro-corticogram (ECoG) measurements (Online Methods). Deeper levels of anesthesia resulted in a loss of all functional responses ($N = 40$; **Supplementary Fig. 11**).

A recent study in the awake rat found that spiking activity of barrel cortex neurons encodes single whisker deflections in a sparse probabilistic way[25]. Our results suggest that this picture should be reconsidered when additional whiskers are engaged in texture detection. Local neurons tuned to antagonist motions fired in a highly reliable way and with precise spiking patterns (**Fig. 5**), well above previously reported values for simultaneous whisker deflections[9,12].

The identification of the sharp antagonist tuning of local neurons was directly derived from the acquisition of a generalized linear-nonlinear model representation including the surround stimulation as an additional dimension. This center-surround interaction model accounts for the neural responses to the whole set of experimental stimuli that we tested on these neurons, including natural patterns of whisker deflections.

We explored this center-surround model for stimulation patterns in which center and surround deflections were delayed with respect to one another. We derived ISI facilitation and suppression curves from these delayed tuning maps comparable to those derived using classical stimulation protocols. These ISI curves displayed facilitation and suppression delays similar to those reported previously and could account for the vast functional variety found in the literature[8,9,27]. In particular, we found that the facilitation and suppression ISI curve depends markedly on the shape of the stimulus (the common subspace phase in our model) and requires a more general representation to characterize the functional role of the neuron.

Recordings targeting the subcortical inputs to the barrel cortex directly will be required to gain a better understanding of the origin of the local-global and simple-complex functional subtypes. Still, we hypothesize that global neurons, which form a large proportion of the neurons recorded in the barrels and in layer V, are the recipient of a subset of ventral posteriomedial (VPM) thalamic neurons. Indeed, layer IV barrels and layer V are the two dominant VPM input areas in the barrel cortex, and there has been increasing evidence that multi-whisker integration could occur in the VPM[38–40]. Another study[23] reported a very strong nonlinear facilitation for the stimulation of three adjacent whiskers, not only in cortex, but also in VPM, suggesting that global-like integrative properties could already be present in VPM.

In contrast with global neurons, local neurons are present in all cortical layers, suggesting a cortical or thalamo-cortical circuit. However, few studies support a role of VPM in the buildup of local neuron properties. Recent experiments have examined the tuning of column C2 neurons to the direction of the motion of a bar crossing the whisker pad in both cortex[28] and thalamus[38]. This tuning is hypothesized to be a result of the subthreshold synaptic input coming from surround barrels rather than thalamus. Indeed, in cortex, 70% of the neurons were tuned to the global stimulus direction, but only 40% in thalamus, and even less after cortical inactivation.

Finally, regarding the simple and complex dichotomy, the linear space described in the thalamus previously[41] does not completely match the phase space found in our study, suggesting that these functional properties emerge at the cortical level. This should be tested in the future.

One limitation of the center-surround model of local neurons is that presumably all surround whiskers do not contribute equally to the response modulation[42], as can be seen at the subthreshold level[3,4,43]. Additional experiments will be necessary to obtain a model that also accounts for this spatial heterogeneity and may predict the functional responses to tactile stimulations with heterogeneous spatial structures. Nevertheless, we expect similar generalized center and surround nonlinear filter representations to exist in other sensory areas in which linear-nonlinear models have been reported to change with the sensory statistics[44], hosting additional coding strategies hidden from classical first-order analyses of the receptive field[35].

METHODS

Methods and any associated references are available in the online version of the paper.

Note: Supplementary information is available in the online version of the paper.

ACKNOWLEDGMENTS

We thank Y. Boubenec for providing the natural whisker stimuli, L. Abbott, L. Bourdieu, A. Davison, V. Ego-Stengel, Y. Frégnac, O. Marre, M. Maravall and H. Sompolinsky for comments on the manuscript, and J. Fournier for advice on the protocol. Funding was provided by ANR (NATACS, HR-CORTEX and TRANSTACT) and the European Community (FET grants FACETS FP6-015879, BrainScaleS FP7-269921 and Brain-i-Nets FP7-243914). S.E.B. was supported by Fondation pour la Recherche Medicale.

AUTHOR CONTRIBUTIONS

L.E. and S.E.B. devised the protocols and analyzed the data with D.E.S. and A.D. L.E. and S.E.B. carried out the extracellular recordings. D.E.S. and A.D. supervised the research. L.E., S.E.B., A.D. and D.E.S. wrote the manuscript.

COMPETING FINANCIAL INTERESTS
The authors declare no competing financial interests.

Published online at http://www.nature.com/doifinder/10.1038/nn.3258.
Reprints and permissions information is available online at http://www.nature.com/reprints/index.html.

1. Carvell, G.E. & Simons, D.J. Biometric analyses of vibrissal tactile discrimination in the rat. *J. Neurosci.* **10**, 2638–2648 (1990).
2. Simons, D.J. Response properties of vibrissa units in rat SI somatosensory neocortex. *J. Neurophysiol.* **41**, 798–820 (1978).
3. Brecht, M. & Sakmann, B. Dynamic representation of whisker deflection by synaptic potentials in spiny stellate and pyramidal cells in the barrels and septa of layer 4 rat somatosensory cortex. *J. Physiol. (Lond.)* **543**, 49–70 (2002).
4. Moore, C.I. & Nelson, S.B. Spatio-temporal subthreshold receptive fields in the vibrissa representation of rat primary somatosensory cortex. *J. Neurophysiol.* **80**, 2882–2892 (1998).
5. Wilent, W.B. & Contreras, D. Dynamics of excitation and inhibition underlying stimulus selectivity in rat somatosensory cortex. *Nat. Neurosci.* **8**, 1364–1370 (2005).
6. Hartmann, M.J., Johnson, N.J., Towal, R.B. & Assad, C. Mechanical characteristics of rat vibrissae: resonant frequencies and damping in isolated whiskers and in the awake behaving animal. *J. Neurosci.* **23**, 6510–6519 (2003).
7. Ritt, J.T., Andermann, M.L. & Moore, C.I. Embodied information processing: vibrissa mechanics and texture features shape micromotions in actively sensing rats. *Neuron* **57**, 599–613 (2008).
8. Ego-Stengel, V., Souza, T.M., Jacob, V. & Shulz, D.E. Spatiotemporal characteristics of neuronal sensory integration in the barrel cortex of the rat. *J. Neurophysiol.* **93**, 1450–1467 (2005).
9. Shimegi, S., Ichikawa, T., Akasaki, T. & Sato, H. Temporal characteristics of response integration evoked by multiple whisker stimulations in the barrel cortex of rats. *J. Neurosci.* **19**, 10164–10175 (1999).
10. Simons, D.J. & Carvell, G.E. Thalamocortical response transformation in the rat vibrissa/barrel system. *J. Neurophysiol.* **61**, 311–330 (1989).
11. Ghazanfar, A.A. & Nicolelis, M.A. Spatiotemporal properties of layer V neurons of the rat primary somatosensory cortex. *Cereb. Cortex* **9**, 348–361 (1999).
12. Hirata, A. & Castro-Alamancos, M.A. Cortical transformation of wide-field (multiwhisker) sensory responses. *J. Neurophysiol.* **100**, 358–370 (2008).
13. Mirabella, G., Battiston, S. & Diamond, M.E. Integration of multiple-whisker inputs in rat somatosensory cortex. *Cereb. Cortex* **11**, 164–170 (2001).
14. Brumberg, J.C., Pinto, D.J. & Simons, D.J. Spatial gradients and inhibitory summation in the rat whisker barrel system. *J. Neurophysiol.* **76**, 130–140 (1996).
15. Schwartz, O., Pillow, J.W., Rust, N.C. & Simoncelli, E.P. Spike–triggered neural characterization. *J. Vis.* **6**, 484–507 (2006).
16. de Ruyter van Steveninck, R. & Bialek, W. Real-time performance of a movement-sensitive neuron in the blowfly visual system: coding and information transfer in short spike sequences. *Proc. R. Soc. Lond. B Biol. Sci.* **234**, 379–414 (1988).
17. de Kock, C.P. & Sakmann, B. Spiking in primary somatosensory cortex during natural whisking in awake head-restrained rats is cell-type specific. *Proc. Natl. Acad. Sci. USA* **106**, 16446–16450 (2009).
18. Geffen, M.N., Broome, B.M., Laurent, G. & Meister, M. Neural encoding of rapidly fluctuating odors. *Neuron* **61**, 570–586 (2009).
19. Maravall, M., Petersen, R.S., Fairhall, A.L., Arabzadeh, E. & Diamond, M.E. Shifts in coding properties and maintenance of information transmission during adaptation in barrel cortex. *PLoS Biol.* **5**, e19 (2007).
20. Skottun, B.C. *et al.* Classifying simple and complex cells on the basis of response modulation. *Vision Res.* **31**, 1079–1086 (1991).
21. Pettigrew, J.D., Nikara, T. & Bishop, P. Responses to moving slits by single units in cat striate cortex. *Exp. Brain Res.* **6**, 373–390 (1968).
22. Lee, S.H. & Simons, D. Angular tuning and velocity sensitivity in different neuron classes within layer 4 of rat barrel cortex. *J. Neurophysiol.* **91**, 223–229 (2004).
23. Ghazanfar, A.A. & Nicolelis, M.A. Nonlinear processing of tactile information in the thalamocortical loop. *J. Neurophysiol.* **78**, 506–510 (1997).
24. Born, R.T. & Tootell, R.B. Segregation of global and local motion processing in primate middle temporal visual area. *Nature* **357**, 497–499 (1992).
25. Jadhav, S.P., Wolfe, J. & Feldman, D.E. Sparse temporal coding of elementary tactile features during active whisker sensation. *Nat. Neurosci.* **12**, 792–800 (2009).
26. Shimegi, S., Akasaki, T., Ichikawa, T. & Sato, H. Physiological and anatomical organization of multi-whisker response interactions in the barrel cortex of rats. *J. Neurosci.* **20**, 6241–6248 (2000).
27. Simons, D.J. Temporal and spatial integration in the rat SI vibrissa cortex. *J. Neurophysiol.* **54**, 615–635 (1985).
28. Jacob, V., Cam, J.L., Ego-Stengel, V. & Shulz, D.E. Emergent properties of tactile scenes selectively activate barrel cortex neurons. *Neuron* **60**, 1112–1125 (2008).
29. Born, R.T. Center–surround interactions in the middle temporal visual area of the owl monkey. *J. Neurophysiol.* **84**, 2658–2669 (2000).
30. Sincich, L.C., Park, K.F., Wohlgemuth, M.J. & Horton, J.C. Bypassing V1: a direct geniculate input to area MT. *Nat. Neurosci.* **7**, 1123–1128 (2004).
31. Pei, Y.C., Hsiao, S.S. & Bensmaia, S.J. The tactile integration of local motion cues is analogous to its visual counterpart. *Proc. Natl. Acad. Sci. USA* **105**, 8130–8135 (2008).
32. Pei, Y.-C., Hsiao, S.S., Craig, J.C. & Bensmaia, S.J. Neural mechanisms of tactile motion integration in somatosensory cortex. *Neuron* **69**, 536–547 (2011).
33. Ferezou, I. *et al.* Spatiotemporal dynamics of cortical sensorimotor integration in behaving mice. *Neuron* **56**, 907–923 (2007).
34. Matyas, F. *et al.* Motor control by sensory cortex. *Science* **330**, 1240–1243 (2010).
35. Jones, H.E., Wang, W. & Sillito, A.M. Spatial organization and magnitude of orientation contrast interactions in primate V1. *J. Neurophysiol.* **88**, 2796–2808 (2002).
36. Newsome, W.T., Wurtz, R.H., Dürsteler, M.R. & Mikami, A. Deficits in visual motion processing following ibotenic acid lesions of the middle temporal visual area of the macaque monkey. *J. Neurosci.* **5**, 825–840 (1985).
37. Rust, N.C., Schwartz, O., Movshon, J.A. & Simoncelli, E.P. Spatiotemporal elements of macaque v1 receptive fields. *Neuron* **46**, 945–956 (2005).
38. Ego-Stengel, V., Le Cam, J. & Shulz, D.E. Coding of apparent motion in the thalamic nucleus of the rat vibrissal somatosensory system. *J. Neurosci.* **32**, 3339–3351 (2012).
39. Aguilar, J.R. & Castro-Alamancos, M. Spatiotemporal gating of sensory inputs in thalamus during quiescent and activated states. *J. Neurosci.* **25**, 10990–11002 (2005).
40. Roy, N.C., Bessaih, T. & Contreras, D. Comprehensive mapping of whisker-evoked responses reveals broad, sharply tuned thalamocortical input to layer 4 of barrel cortex. *J. Neurophysiol.* **105**, 2421–2437 (2011).
41. Petersen, R.S. *et al.* Diverse and temporally precise kinetic feature selectivity in the VPm thalamic nucleus. *Neuron* **60**, 890–903 (2008).
42. Le Cam, J., Estebanez, L., Jacob, V. & Shulz, D.E. Spatial structure of multi-whisker receptive fields in the barrel cortex is stimulus dependent. *J. Neurophysiol.* **106**, 986–998 (2011).
43. Zhu, J.J. & Connors, B.W. Intrinsic firing patterns and whisker-evoked synaptic responses of neurons in the rat barrel cortex. *J. Neurophysiol.* **81**, 1171–1183 (1999).
44. Touryan, J., Felsen, G. & Dan, Y. Spatial structure of complex cell receptive fields measured with natural images. *Neuron* **45**, 781–791 (2005).

ONLINE METHODS

Animal preparation and electrophysiology. Experiments were performed in conformity with French (Comite d'ethique en matiere d'experimentation animale Paris Centre et Sud) and European (86/609/CEE) legislation. Male Wistar rats (N = 68, 302 ± 15 g) were deeply anesthetized (stage III, plane 3) with 3% isoflurane in 1 l min^{-1} 80% N_2O / 20% O_2 and placed in a stereotactic frame. Body temperature was maintained at 37 °C with a feedback-controlled heating pad. The left postero-medial barrel subfield was exposed. Following surgery, isoflurane concentration was progressively adjusted (2.5 to 0.6%) to maintain the rat in a lightly anesthetized state (stage III, plane 1–2) based on three criteria: fast ECoG (≥5 Hz) oscillations, a stable 1–1.5-Hz respiration rate and a lack of spontaneous movements[45]. After removing the dura, 32 channel silicon probes (Neuronexus, recording size = 177 μm^2, 4 and 8 shank geometries) were inserted in the cortex. Spike sorting of single units was performed manually using Offline Sorter (Plexon) on the space defined by the first two dimensions of the PCA of spikes shapes. Spike clusters that were clearly separated from the noise cluster were isolated. They were retained as units if the autocorrelogram displayed at least a 1-ms refractory period and the spike shape was physiological and consistent through the cluster. We allowed only a limited drift of the spike shape amplitude during the hour-long recordings. These criteria resulted in a set of units that displayed waveform signal-to-noise ratios (SNRs; that is, the peak-to-peak amplitude of the smallest waveform for a given unit, divided by the r.m.s. of the noise) ranging from 3.1 to 25, and 98% of all waveforms displayed a SNR above 4.0. The mean SNR was 6.7 and the median SNR 6.2.

Multi-whisker stimulation. The 24 most caudal right whiskers of the rat were simultaneously and independently deflected in the rostro-caudal axis using a custom-built multi-whisker stimulator, allowing the design of various tactile scenes[46]. Whiskers were cut to a length of 10 mm and inserted 5 mm into each whisker stimulator. The resting angle of each whisker was used as the stimulation's zero position (**Supplementary Fig. 1a**).

The stimulus used to carry out the reverse correlation analysis was built by linking with a quadratic spline a series of points extracted from a Gaussian distribution (s.d. = 75 µm) and set every 5.5 ms apart. The resulting white noise displayed a bandwidth of 82 Hz and was well reproduced by the piezoelectric actuators, as verified by measuring the level of correlation between the command and actual motion (r = 0.991; **Supplementary Fig. 1b,c**) with a laser telemeter (MicroEpsilon). No noticeable ringing was present in the actuator motion. The amplitude and speed of this stimulation (3.6° range and 590° s^{-1} peak speed) matched the range of values observed during contacts with textures in freely behaving rats[25,47].

The stimulus was applied simultaneously across the whisker pad at different interwhisker correlation levels, from 0 to 100%. A center-surround version of this stimulus was obtained by applying two uncorrelated stimuli, one to the principal whisker of the neuron (previously identified using an on-line classical sparse noise characterization of the receptive field) and another to the remaining surround whiskers. Each recording session was 4 h long and was built by randomly combining 10-s epochs of the different protocols. Quadratic splines linkage of the successive epochs ensured that the stimulation was constantly dense and smooth across the whole recording.

An additional stimulus was designed in which the calculated filters from the previous stimulus protocol were played back with the stimulation matrix and forward correlation analysis was applied to the neuronal activity. We built this stimulus by combining repetitions of the first common filter. This filter was randomly replayed in both directions, separated by Poisson-like intervals (λ = 40 ms, refractory period = 46 ms). A correlated condition was generated by replaying the same realization on all whiskers, an uncorrelated version was obtained by applying different realizations on each whisker and an antagonist condition was obtained by inverting the direction of the center whisker in the correlated stimulus.

Finally, to test our models, we stimulated the 24 whiskers with natural whisker deflections acquired with high-speed videography (500 Hz) during the sweeping of a rough texture through the whisker pad of an anesthetized rat. These 10-s-long whisker deflections were Bessel filtered to fit the 0.1–83-Hz bandwidth of the whisker stimulator (**Fig. 5g,h**).

Histology. In half of the experiments (32 of 63), before the first recording, DiI stain was deposited on the shanks of the electrode[48]. At the end of the recordings, rats were killed by pentobarbital overdose and transcardially perfused. The left postero-medial barrel subfield was flattened. We tangentially cut 46-µm-wide slices and stained them with cytochrome oxidase to visualize layer IV barrels (**Supplementary Fig. 8a**). A three-dimensional reconstruction of the electrode and barrels was performed using Trakem2 (**Supplementary Fig. 8b**)[49]. Both the lateral positioning of the electrode recording points in the barrel cortex (barrel versus septum) and the depth of the recordings was inferred from this reconstruction (N = 159; **Supplementary Fig. 8c**). For reference, we also provide the distribution of recording depths as reported by the micromanipulator holding the electrode for all recorded neurons (N = 429; **Supplementary Fig. 8.d**).

Analysis of neuronal data. Reverse correlation analysis was applied on the data collected during Gaussian noise stimulations, while data collected during discrete playback, sparse noise or natural stimulations experiments were analyzed by building PSTHs. To construct the spike-triggered ensemble, peri-spike whisker deflection waveforms were collected in the time interval [−40 ms, +10 ms] relative to the spike and binned at 2-ms resolution, so that each whisker's ensemble was defined over 25 dimensions.

STC analysis was only carried out on recordings with at least 50 spikes per stimulus dimensions[37] unless a spike-triggered average was accurate enough to describe the cell functional properties (in which case a minimum number of 750 spikes were required per protocol). This was the case for simple cells, which generally had a smaller firing rate as a result of their sharp sensory selectivity and their lower baseline activity. As a result of the combination of the very short response latencies seen in this system[43] (as early as 5 ms) and the approximately 10-ms-long autocorrelation of the Gaussian noise stimulus, some neurons displayed filters that artifactually extended in positive times by up to 2–4 ms.

In the case of correlated or anticorrelated stimulations, there are only one or two spatial dimensions, indicating that the minimal spike counts were 1,250 and 2,500 spikes, respectively. In the case of uncorrelated stimulations, a direct analysis of the full receptive field with 25 time bins would have required 32,000 spikes. To avoid this constraint, given that the time course of the linear filters is only interesting in the case of whiskers that trigger significant responses, we only carried out a full STC analysis on significant whiskers. To this end, we split the analysis into two steps for uncorrelated stimulations. We first evaluated the significance of the response to each whisker using spike-triggered average and the diagonal of the STC. This first step was systematically confirmed by comparing it with the outcome of forward correlation analysis playback protocols. On the few identified significant whiskers (up to three), we then carried out the full STC analysis. This analysis required at least 3,750 spikes if the neuron displayed three significant whiskers and 1,250 spikes for one whisker. The distribution of spike count per protocol for neurons analyzed with STC ranged from 1,250 to 57,570 spikes with a mean value of 6,700 ± 8,777 (s.d.).

The spike-triggered ensembles of whisker stimulations were whitened by multiplication with the inverse of the stimulus covariance matrix to remove spatial and temporal correlations. Spatial correlations were obtained in our protocol by adding a common Gaussian noise signal to all whiskers (**Fig. 3**) so that the overall stimulation remained Gaussian and thus allowed a consistent estimation of the linear-nonlinear model. The covariance matrix corresponding to this spatial correlation is basically an identity matrix with the correlation coefficient in the off-diagonals corresponding to instantaneous correlation with other whiskers.

The stimulus space is not only affected by various levels of spatially homogeneous correlation, but is also conditioned by the bandwidth of the stimulus (0–83 Hz, 3-dB bandwidth). This bandwidth was selected to stay in the linear regime of the actuator to avoid any resonance or excessive fatigue (**Supplementary Fig. 1**). To obtain this bandwidth, the stimulus was built by linking a discrete version of the Gaussian noise signal with splines, resulting in temporal correlations. To partially correct this loss of high frequencies and the additional time correlation, we applied a ridge regression with a homogeneous parameter $\lambda = 5.5 \times 10^5$ on the stimulus covariance matrix. This allowed us to compute the pseudo-inverse matrix that was used to rectify the spectrum for high frequencies[50]. This regularization was applied to all mono-whisker filters and provided a better estimation of a neuron's preferred frequency than the raw spike-triggered analysis, thanks to the wider sampled frequency band (**Supplementary Fig. 2**). It is worth noting that the functional cell type (local-global and simple-complex) is not affected by this regularization, which mainly affects the neuron overall sensitivity to sensory input as well as its frequency tuning.

doi:10.1038/nn.3258

STC analysis was then carried out first by computing the mean covariance matrix over the whitened spike-triggered ensemble, and second by applying singular value decomposition on the resulting matrix to find eigenvalues and eigenvectors (linear filters). Significant eigenvectors were determined by comparing the corresponding eigenvalues with significance thresholds derived from a pool of 200 surrogates, randomly time-shifted spike trains[44]. Linear filters were considered significant when their corresponding eigenvalue exceeded the surrogate distribution mean value by at least eight s.d. (z score). Finally, the nonlinear function of the linear-nonlinear model was computed as the ratio between the spike-triggered ensemble distribution and the prior distribution on the subspace corresponding to the significant eigenvectors, multiplied by the mean firing rate[15]. This is written as a Bayesian equation

$$P(\text{spike}|\text{stimulation}) = \frac{P(\text{spike})\,P(\text{stimulation}|\text{spike})}{P(\text{stimulation})}$$

where P(spike) is the neuron firing rate, P(stimulation|spike) is the spike-triggered stimulation distribution and P(stimulation) is the prior distribution irrespective of the spike times.

To assess the demarcation between common filters 1 and 2 and the additional linear filters (**Fig. 1c**), we computed the average over 40 PCA eigenvalues, which were each computed from a pool of 680 noise filters built from random spike times (same filter counts as in **Fig. 1e**). Only filters 1 and 2 were more than threefold larger than the s.d. (**Fig. 1c**), a threshold that is classically regarded as significant.

The center-surround linear-nonlinear model was obtained by convolving the center and surround inputs (x_c and x_s) with the common linear filters f, and by combining the result into a single center-surround nonlinear function R. This four-dimensional function described in polar coordinates (radius r and phase θ for both the center and surround stimulus projections) was reduced to a two-dimensional tuning map, R', by expressing the radial parts as a separated radial function

$$\text{Output} = R(f * x_c, f * x_s) = R(r_c, r_s, \theta_c, \theta_s) = \left[R'(\theta_c, \theta_s) \cdot \left(\alpha_c \cdot r_c^2 + \alpha_s \cdot r_s^2 \right)^{1/2} - r_{th} \right]_+$$

where all parameters could be obtained directly from the data by considering separately the phase tuning and the radius dependency. This model structure was inspired by a previous study in the visual cortex[37]. This model was used to fit neuron responses to predict PSTHs obtained with natural stimuli (with a 20-ms tim bin) and playbacks (**Fig. 5c**,**d**,**g**–**j**). For these predictions, we fitted an additional scaling parameter to account for the change of variance (compared with Gaussian noise) that has been shown to affect the scaling of the nonlinear function[20] (**Supplementary Fig. 12**). The exact same model was used to predict correlated and center-surround stimulations. The same procedure was also used to predict the PSTH obtained with uncorrelated natural stimulation (**Supplementary Fig. 8**).

To obtain the simple-complex modulation ratio R_1/R_0 from the data or the linear-nonlinear model obtained for uncorrelated Gaussian noise, we evaluated the power spectral density of the neuron response for an oscillating input at a 50-Hz frequency. Stimuli used on the whisker pad were sinusoidal functions that were identical for all whiskers in the same column and anti-phased from one column to the next to mimic a drifting grating (usually used in V1). R_1 corresponds to the PSTH spectrum amplitude for the driving frequency (50 Hz), whereas R_0 corresponds to the non-oscillating (DC) spectrum amplitude (0 Hz).

Firing probability (**Fig. 5**) was computed as the ratio between the number of trials in which the cells fired in a time window delimited by the PSTH width at mid-height and the total number of trials. The PSTH average z score used in **Figure 6** was computed across a 20-ms time window centered on the maximal rate found in the time interval [0 ms, 100 ms]. The average PSTHs shown in **Supplementary Figure 10** were computed similarly, but without the z score.

45. Friedberg, M.H., Lee, S.M. & Ebner, F.F. Modulation of receptive field properties of thalamic somatosensory neurons by the depth of anesthesia. *J. Neurophysiol.* **81**, 2243–2252 (1999).
46. Jacob, V. *et al.* The Matrix: a new tool for probing the whisker-to-barrel system with natural stimuli. *J. Neurosci. Methods* **189**, 65–74 (2010).
47. Wolfe, J. *et al.* Texture coding in the rat whisker system: slip-stick versus differential resonance. *PLoS Biol.* **6**, e215 (2008).
48. DiCarlo, J.J., Lane, J.W., Hsiao, S.S. & Johnson, K.O. Marking microelectrode penetrations with fluorescent dyes. *J. Neurosci. Methods* **64**, 75–81 (1996).
49. Cardona, A. *et al.* An integrated micro- and macroarchitectural analysis of the *Drosophila* brain by computer-assisted serial section electron microscopy. *PLoS Biol.* **8**, e1000502 (2010).
50. Smyth, D., Willmore, B., Baker, G.E., Thompson, I.D. & Tolhurst, D.J. The receptive-field organization of simple cells in primary visual cortex of ferrets under natural scene stimulation. *J. Neurosci.* **23**, 4746–4759 (2003).